



Effect of rheological properties of potato, rice and corn starches on their hot-extrusion 3D printing behaviors

Huan Chen^a, Fengwei Xie^{b,c}, Ling Chen^{a,*}, Bo Zheng^{a,**}

^a Ministry of Education Engineering Research Center of Starch & Protein Processing, Guangdong Province Key Laboratory for Green Processing of Natural Products and Product Safety, School of Food Science and Engineering, South China University of Technology, Guangzhou, 510640, China

^b Institute of Advanced Study, University of Warwick, Coventry, CV4 7HS, United Kingdom

^c International Institute of Nanocomposites Manufacturing, WMG, University of Warwick, Coventry, CV4 7AL, United Kingdom

ARTICLE INFO

Keywords:

Hot-extrusion 3D printing

Rheological property

Printing behavior

Potato starch

Rice starch

Corn starch

Chemical compounds:

Starch (PubChem CID: 24836924)

Sodium hydroxide (PubChem CID: 14798)

Water (PubChem CID: 962)

Ethanol (PubChem CID: 702)

Acetic acid (PubChem CID: 176)

Iodine (PubChem CID: 807)

Potassium iodine (PubChem CID: 4875)

ABSTRACT

In this study, the relationship between rheological properties and printability of three types of starch (potato, rice and corn starch) for hot-extrusion 3D printing (HE-3DP) were systematically investigated. Each starch sample showed a shear-thinning behavior, self-supporting property, as well as the feature of a substantial decrease at higher strains and a recovery at lower strains in storage modulus (G'), which indicated the suitability of starch for HE-3DP. Besides, the flow stress (τ_f), yield stress (τ_y), and G' increased with a higher starch concentration. We found that starch suspensions with concentrations of 15–25% (w/w) heated to 70–85 °C possessed preferable values of τ_f (140–722 Pa), τ_y (32–455 Pa), and G' (1150–6909 Pa) for HE-3DP, which endowed them with excellent extrusion processability and sufficient mechanical integrity to achieve high resolutions (0.804–1.024 mm line width). Overall, our results provided useful information to produce individualized starch-based food by HE-3DP.

1. Introduction

Emphasis has been placed on the diversification and personalization of food to meet the special demands of particular groups of consumers such as the elderly, children and athletes. Given this, 3D printing technologies have been introduced and adapted to meet the demand of food design and related food materials processing. Food 3D printing, also known as food layered manufacturing (Wegrzyn et al., 2012; Yang et al., 2017), is capable of eliminating the requirement of particularly shaped molds and potentially offers a much wider design space beyond unusual shaping (Kokkinis et al., 2015). Moreover, 3D printing technology can also revolutionize food manufacturing by the ability to fabricate 3D constructs with complex geometries, elaborated textures, and tailored nutritional contents (Sun et al., 2015). Among all food 3D printing technologies, extrusion 3D printing, especially hot-extrusion 3D printing (HE-3DP), has drawn much attention due to its ability to deposit ingredients to solid geometries (Long et al., 2017). HE-3DP involves extruding a molten or semi-solid material through a small-diameter nozzle moving along the X- and Y-directions, and the printing

platform moves down in the Z-direction for the deposition of the next layer (Jafari et al., 2000).

A series of preferable properties of printing media for HE-3DP includes the ease of loading into the printer syringe and extruding from its fine nozzle, the sufficient mechanical integrity of printed threads to support stacked layers without printing defects such as buckling and sagging, and the high stability of threads after their deposits to ensure a good resolution of the printed object. All of these properties can be well reflected by the rheological behaviors of printing media. Specifically, the printing media should be shear-thinning and with suitable flow stress to be easily extruded from the fine nozzle (Duoss et al., 2014; Le Tohic et al., 2018). Furthermore, the printing media should be not only viscoelastic but also elasticity-dominant ($\tan \delta < 1$), and have high yield stress to avoid the inconsistent printing from broken threads. More importantly, the media should present a rapid and reversible modulus response to shear stress to ensure a good resolution of printed objects (Zhang et al., 2015). Given this, the rheological properties of printing media are critical for their HE-3DP (Hong et al., 2015; Liu et al., 2018).

* Corresponding author.

** Corresponding author.

E-mail addresses: 201710104198@mail.scut.edu.cn (L. Chen), zhengbo0522@126.com (B. Zheng).

Abbreviations

HE-3DP	hot-extrusion 3D printing
G'	storage modulus
G''	loss modulus
$\tan \delta$	loss tangent

τ_f	flow stress
τ_y	yield stress
RS	rice starch
PS	potato starch
CS	corn starch

Starch, as one of the most important carbohydrates in human diets, has been extensively used in food applications to improve the process convenience and the quality of final products (Zheng et al., 2018). In food systems, starch often undergoes gelatinization during cooking. During this process, starch granules swell extensively with the resultant disrupted crystalline structure. Meanwhile, amylose molecules diffuse out from the swollen granules (Wang et al., 2018). As a result, starch pastes can be regarded as a continuous matrix of entangled amylose molecules reinforced by embedded swollen granules (Ring, 1985). This particular structural feature endows the gelatinized starch paste with viscoelasticity, which shows a shear-thinning behavior and instant responses to the applied shear strains (Evans and Haisman, 1980). Regarding this, starch shows high potential for HE-3DP.

Despite the huge advantages of HE-3DP technology, research in food printing has just been started. Various food materials have been used to print a complex structure, such as chocolates (Lanaro et al., 2017), confections (Hao et al., 2010), proteins, meat purees, and other nutrients (Cohen et al., 2009; Lipton et al., 2010; Serizawa et al., 2014). These printable food materials either are based on its own thermal characteristics (typically, melting upon heating and solidification on cooling) or need further modification to acquire printability. There is limited data about the 3D printing of grain-based food, which highly hampers the application of 3D printing in the production of next-generation daily dietary food since the major ingredients of most snack foods are grain-based. Only a few studies have concerned 3D printed grain-based products based on, for instance, mashed potato products with different contents of potato starch (Liu et al., 2018). Also, potato starch was reported to adjust the rheological properties of lemon juice gels in order to develop new 3D printed food constructs in lemon juice gel systems (Yang et al., 2018). Still, this field is in its infancy and the improvement of the currently developed systems is urgently needed. Therefore, motivated by the excellent rheological properties of starch, this study focuses on the rheological behaviors of rice starch (RS), potato starch (PS), and corn starch (CS) under the conditions mimicking the HE-3DP process, and their actual printing behaviors. The aim of this work is to illuminate the underlying relationship between starch rheological properties and printability, and provide insights into the 3D printing of starch-based staple food.

2. Materials and methods

2.1. Materials

RS was supplied by National Starch Pty Ltd. (Lane Cove, NSW, 2066; Australia). CS was obtained from Huanglong Food Industry Co., Ltd. (P. R. China). PS was provided by Sanjiang Group Co., Ltd. (Xining, China). Anhydrous ethanol was supplied by Nanjing Chemical Reagents Co., Ltd. (Nanjing, China). Sodium hydroxide was obtained from Tianjin Baishi Chemical Co., Ltd. (Tianjin, China). Iodine and Potassium iodine were purchased from Sinopharm Chemical Reagent Co., Ltd. (Beijing, China). Acetic acid was provided by Jiangsu Qiangsheng Chemical Co., Ltd. (Jiangsu, China). Potato amylose and rice amylopectin were purchased from the Heilongjiang Academy of Agricultural Sciences (Harbin, China).

2.2. Main components analysis

The apparent amylose contents of starch samples were determined by using the AACC method 61–03(10) with minor modification. 100 mg of dry starch was dispersed in 1 mL of anhydrous ethanol and 9 mL of 1 M NaOH solution, and completely dissolved by heating at 100 °C for 10 min with shaking. Then, the starch solution was diluted with water into 100 mL after cooling to the ambient temperature. 2.5 mL of this diluted solution was mixed with 25 mL of water, then added with 0.5 mL of 1 M acetic acid solution and 0.5 mL of 0.2% iodine solution, and made up to 50 mL with water. A UV-3802 spectrophotometer (UNICO, New Jersey, USA) was used to measure the absorbance at 620 nm. The amylose content values were calculated from a standard curve established using mixture solutions of amylose and amylopectin ($R^2 = 1$). A moisture analyzer (MA35, Sartorius Stedim Biotech GmbH, Germany) was used to determine the moisture content of the original starch. The amylose and moisture contents were given in Table 1.

2.3. Sample preparation

A series of homogeneous starch suspensions were prepared at 5, 10, 15, 20, 25 and 30% (w/w, dry basis) concentrations using a procedure reported before (Keetels et al., 1996).

2.4. Rheological measurements

Dynamic mechanical parameters (storage modulus (G'), loss modulus (G''), and loss tangent ($\tan \delta$)) were used to evaluate the viscoelastic properties of starch samples on an Anton Paar MCR 302 rheometer. For each measurement, a certain concentration of starch suspension was loaded between the stainless steel parallel plates (with a diameter of 25 mm and a gap of 1 mm) and equilibrated at a certain starting temperature. The exposed edges of the samples were covered with a thin layer of silicon oil to prevent moisture evaporation.

Temperature sweeps were undertaken from 45 °C to 100 °C at a rate of 2 °C/min, and the strain and frequency were set at 0.5% and 10 rad/s, respectively.

For oscillation tests, starch suspensions were heated from 45 °C to a certain temperature (RS to 80 °C, PS to 70 °C, and CS to 75 °C) at 5 °C/min and kept at the temperature for 5 min. Strain sweeps were first conducted at a frequency of 10 rad/s to obtain strain values in the linear viscoelastic region. Yield stress (τ_y) was measured under oscillatory stress sweep at a frequency of 10 rad/s. Alternate strain sweep tests were performed using alternating strains of 1% (in the linear viscoelastic region) for 2 min and 100% (beyond the linear viscoelastic region) for 2 min per cycle at a frequency of 10 rad/s to investigate the response of G' to strain of the starch samples.

Table 1
Amylose and moisture contents of PS, CS and RS.

Variety	Amylose Content (%)	Moisture (%)
PS	34.5 ± 0.4	15.54 ± 0.03
CS	24.1 ± 0.6	14.59 ± 0.01
RS	26.5 ± 0.3	14.97 ± 0.05

Steady shear rheological measurements were undertaken using the same facility with a 40-mm cone-and-plate geometry. Viscosity was recorded with a shear rate range from 0.1 to 100 s⁻¹.

2.5. HE-3D printer and HE-3DP process

Fig. 1 shows the schematic of the HE-3D printer SHINNOVE S2 (Shiyin Tech Co., Ltd., Hangzhou, China). The system includes four parts: (1) the rack and pedestal; (2) information and control display; (3) an annular electric heating tube outside the feed cylinder combined with a temperature sensor, which could regulate the temperature from 20 °C to 200 °C; a stepper motor system is computer-controlled and synchronized with the movement of the feed cylinder with an extruding head in the X-Y directions and the printing platform in the Z direction to ensure precise deposition and object buildup; (4) a feed cylinder that stores a printing medium. Printing requirements and models could be chosen through the display control panel or a mobile terminal. A 0.8-mm diameter nozzle was used and the nozzle height was set at 2.0 mm, which can affect the printing accuracy significantly by limiting the space within which the extruded mixtures can flow. A nozzle speed of 20 mm/s and an extrusion rate of 30 mm/s were used to obtain desired results according to our preliminary work. The prepared starch suspension was poured into the feed cylinder, heated to a required temperature, and held for 5 min to reach equilibrium, and then a preferred model was chosen to start the printing.

The width of printed lines was measured with an optical microscope on a printed square model (60 × 60 mm). The highest layer numbers were recorded by printing the bowl model (28 × 28 × 49 mm) that can be extruded from the nozzle smoothly and without collapse.

2.6. Statistical analysis

All the experiments were performed at least in triplicate, the mean values and differences were analyzed using Duncan's multiple-range test. Analysis of variance (ANOVA), followed by the least significant difference test (LSD-test), was performed using SPSS (Version 22.0) software. The significance level was set at $p < 0.05$.

3. Results and discussion

3.1. Steady shear rheological study

An ideal printing medium for extrusion through a small-diameter nozzle in HE-3DP is a shear-thinning material to ensure smooth extrusion (Zhang et al., 2015). To understand the viscoelasticity of starch suspensions as HE-3DP printing media, steady shear rheological measurements were carried out and the results are shown in Fig. 2. A linear relationship between viscosity and shear rate can be seen on the double logarithmic plot for CS at 75 °C, RS at 80 °C and PS at 70 °C of various concentrations (5–30%, w/w), indicating that in all these cases, the power-law model is applicable to describe the rheological behavior (Chen et al., 2017; Suzlin et al., 2011; Xie and Shao, 2009).

$$\eta = K\dot{\gamma}^{n-1} \quad (1)$$

Where η is the viscosity (Pa·s) of starch systems, $\dot{\gamma}$ is the shear rate (s⁻¹), K is the consistency (Pa·s), and n is the power-law index. For a pseudo-plastic solution, $n < 1$.

The detailed parameters of regression power-law equations for different starch samples were listed in Table 2. It can be seen that nearly all correlation coefficients (R^2) were close to 0.999, showing a strong power-law dependence of viscosity on shear rate. In addition, all n values were much lower than 1, indicating all starch samples strongly behaved as a non-Newtonian fluid and showed a shear-thinning behavior. For each starch, the viscosity increased with the increased concentration at the same shear rates. Moreover, at concentrations of 10% (w/w) or lower, the viscosity value of PS was highest followed by RS

and CS at the shear rate from 0.1 to 100 s⁻¹, while at higher concentrations (15–30% (w/w)), the highest value was RS. This was in agreement with the trend of G' during temperature sweep (discussed below).

3.2. Dynamic shear rheological study

3.2.1. Temperature sweep

The viscoelastic property of starch suspension can be reflected by both G' and $\tan \delta$ (Caldirola, 1962; Li and Yeh, 2001). Thus, it is essential to choose proper temperatures to acquire gelatinized starch samples with sufficient G' and $\tan \delta$ to respond to the elastic deformation thus to support more printed layers during the deposition process of HE-3DP.

Fig. 3 presents the changes in G' (A) and $\tan \delta$ (B) as a function of temperature for PS, RS and CS suspensions (10–30%, w/w) during temperature sweep at 2 °C/min. All starches exhibited similar profiles during temperature sweep (Fig. 3 (A)). Specifically, at low temperatures, G' remained low and unchanged as starch could not dissolve in cold water. As the temperature increased and reached a certain point (T_G), G' increased dramatically along with a sharp decrease in $\tan \delta$ (Fig. 3 (B)) because of the closely packed matrix caused by the swelling of starch granules (Lii et al., 1996). Furthermore, the increased temperature led to an increase in G' to a maximum (G'_{max}) at $T_{G'_{max}}$, which was as expected and is consistent with previous studies (Ji et al., 2017; Li and Yeh, 2001). This indicates that heating could not only promote the swelling of starch granules and make amylose leach out, but also increase the mobility and collision of swollen granules and amylose molecules to form a special 3D conformation. All these contributed to an increase in G' (Lii et al., 1995; Wong and Lelievre, 1981). After reaching G'_{max} , G' reduced dramatically with further heating, which was in accordance with previous research (Ji et al., 2017; Keetels et al., 1996). This drop in G' could be attributed to the rupture of starch granules, the breakage of the intermolecular interactions (typically hydrogen bonding), and the reduction in the degree of chain entanglements (Lii et al., 1996).

Table 3 lists the $T_{G'_{max}}$, G'_{max} and $\tan \delta_{G'_{max}}$ values for all the cases during temperature sweeps. It can be seen that an increase in concentration could result in higher G'_{max} for all the starches. Especially, RS displayed higher G' and lower $\tan \delta$ than PS and CS at concentrations of 15–30% (w/w). This could be explained by the reinforced rigidity of RS granules caused by the lower swelling capacity and deformability of RS compared with PS and CS (Singh et al., 2003), since the swollen starch granule was the major factor for the viscoelastic properties of heated starch systems (Lii et al., 1996; Svegmarm and Hermansson, 1991; Tsai

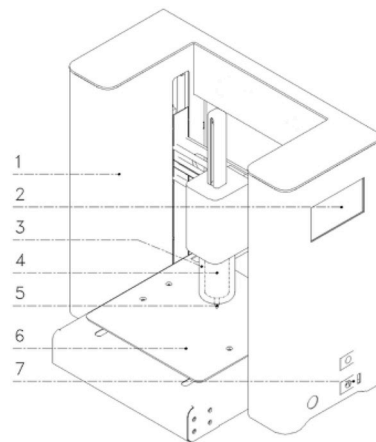


Fig. 1. Schematic of the HE-3D printer used in this work. 1) Rack; 2) Information and control display; 3) Heating tube; 4) Feed cylinder; 5) Extruding head; 6) Printing platform; 7) USB and SD card slot.

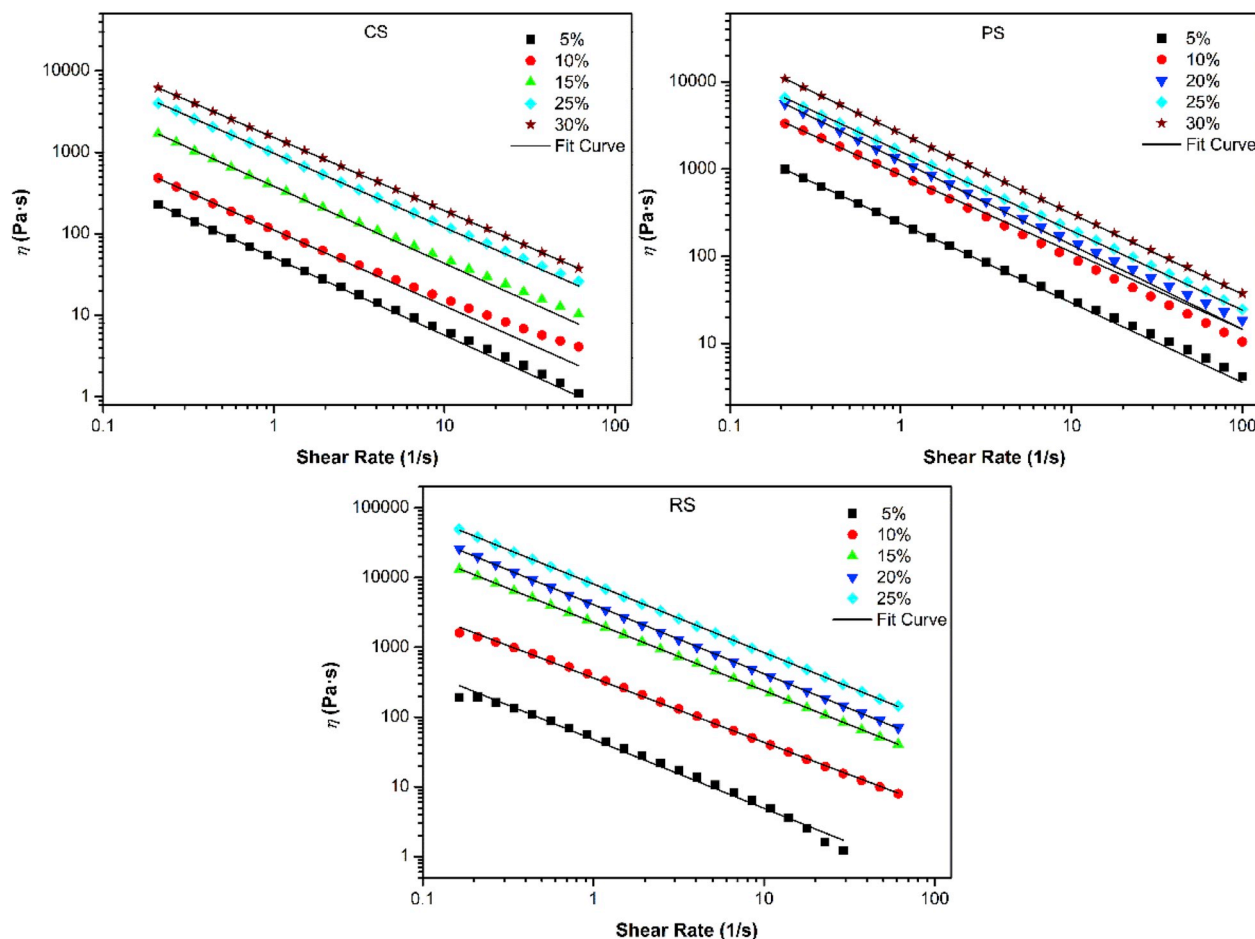


Fig. 2. Viscosity versus shear rate profile for starch samples at different concentrations.

Table 2
Power-law parameters for starches of different concentrations.

Variety	Concentration (w/w)	n	K (Pa·s)	R ²
RS	5%	0.235 ^a	54.7 ^e	0.983
	10%	0.200 ^b	398.9 ^d	0.996
	15%	0.034 ^c	2304.4 ^c	0.999
	20%	-0.032 ^d	4000.4 ^b	0.999
	25%	-0.009 ^e	7974.2 ^a	0.999
CS	5%	0.047 ^a	51.1 ^e	0.999
	10%	0.068 ^a	111.5 ^d	0.999
	15%	0.053 ^a	382.7 ^c	0.999
	25%	0.089 ^a	972.9 ^b	0.999
	30%	0.102 ^a	1520.2 ^a	0.999
PS	5%	0.089 ^{ab}	238.8 ^e	0.999
	10%	0.116 ^a	856.0 ^d	0.999
	20%	0.035 ^c	1242.9 ^c	0.999
	25%	0.092 ^b	1585.6 ^b	0.999
	30%	0.078 ^b	2567.9 ^a	0.999

Superscripts with different letters in the same column indicate significant differences ($p < 0.05$).

et al., 1997). Also, it has been suggested that starch suspension with $G' > 500$ Pa and $\tan \delta < 0.2$ during the temperature sweep could be considered as an elastic gel (Lii et al., 1995). Thus, RS was much stiffer than PS and CS systems and tended to show gelling behavior during heating. Therefore, compared with PS and CS, RS was more preferable as an HE-3DP material since the gel-like characteristics are critical for the printing medium to be dispensed as a free-standing filament (Chung et al., 2013; Cohen et al., 2009).

3.2.2. Alternate strains sweep

When being extruded from and out of the nozzle, a printing medium will undergo a high-shear process and a low-shear process sequentially, thus materials for extrusion 3D printing should not only be easily extruded from the nozzle but also maintain sufficient mechanical integrity when being extruded out of the nozzle to support the next printed layer (Liu et al., 2018). To further understand the responsiveness of starch systems to shear strain, CS, RS and PS (10–30% (w/w)) were subjected to two cycles of low (1%) and high (100%) strains for 2 min, respectively.

Fig. 4 shows a reversible nature of the physical entanglement networks of starch samples manifesting themselves in the instantaneous response of G' to the applied alternate strains. All the starch samples exhibited a remarkable decrease in G' at high strains and instant recovery at low strains. According to the polymer conformational change theory (Shaw, 2011), the flexible starch macromolecular chains are orientated along the flow direction under an external stress with the resulting reduced conformational entropy of the polymer system. Once the external force is removed, the conformational entropy will partially restore. Thus, the decrease in G' for all the three starch samples at a high shear strain could be attributed to the disruption of the physical network due to the macromolecular chains orientation. Subsequently, the rapid recovery in G' at low shear strains was related to the rapid reformation of the transient network, which was promoted by the partially or fully restored conformation due to the reconstruction of the physically entangled structure (Winnik and Yekta, 1997).

Table 4 lists the G' values at different stages during alternate strains sweep tests. G'_1 corresponds to G' during the temperature sweep. It was found that all the starch samples remarkably decreased to G'_2 and

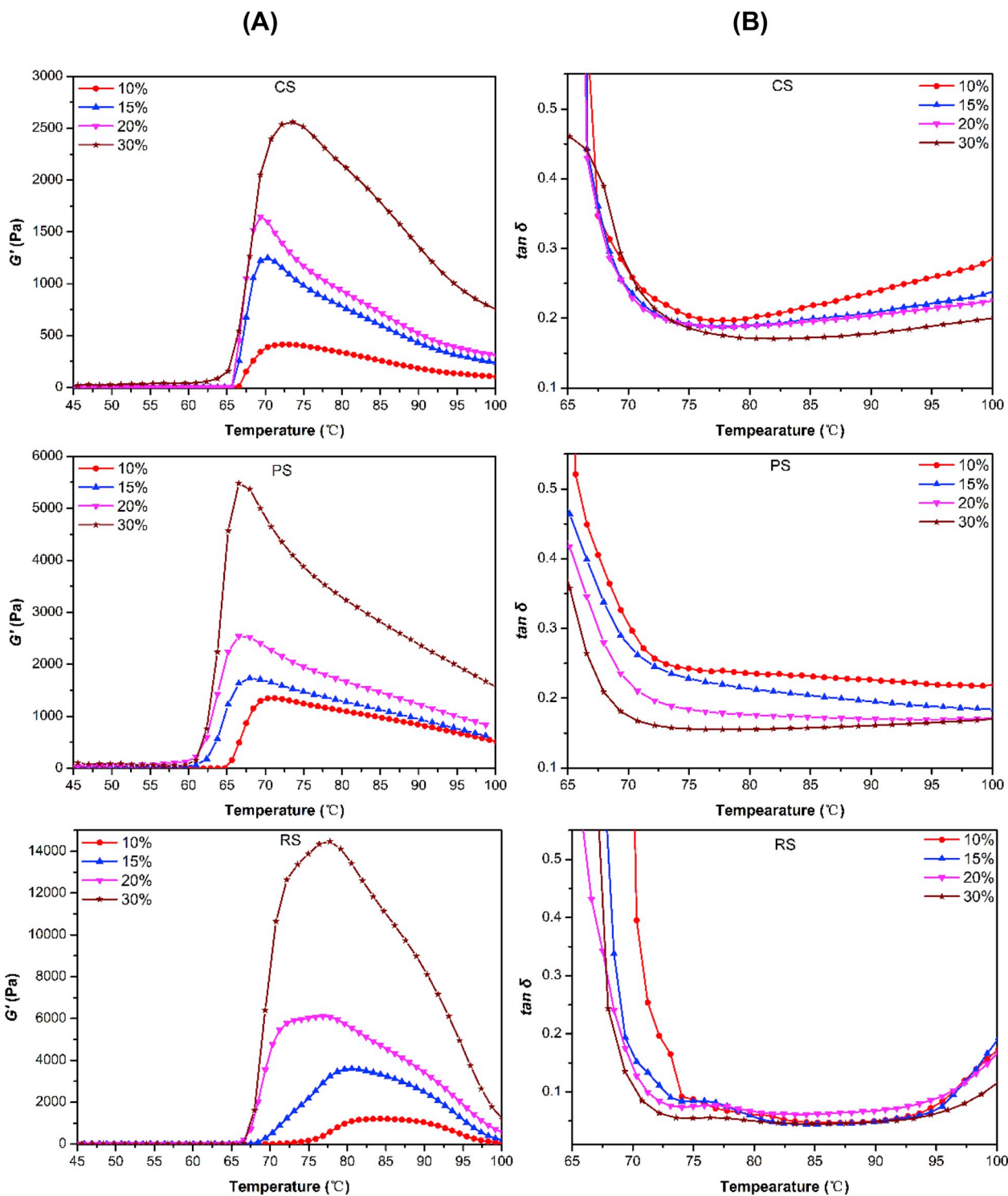


Fig. 3. Storage modulus (G') (A) and $\tan \delta$ (B) as a function of temperature during dynamic oscillatory temperature sweep for PS, RS and CS suspensions at different concentrations.

displayed an apparent decline from G'_1 to G'_3 . This small hysteresis between the G'_1 and G'_3 could result from the higher G'_1 in the first stage caused by the initial equilibration at 0% strain. Another reason may be the non-total recovery of the physically entangled network structure under the high strain, which would lead to lower G'_3 . Yet, a less reduction from G'_3 to G'_5 was shown, indicating that all the starch samples could instantly restore to the previous structure at low strains after a high shear process. This desirable property of rapid and

reversible modulus responding to shear strain shows the suitability of these starch materials for HE-3DP.

3.2.3. Stress sweep

Fig. 5 (A) shows the corresponding stress sweep results for 20% (w/w) starch samples. It can be noticed that RS had the highest G' values, followed by PS and then CS, which was corresponding to the temperature sweep results. The results showed that CS, PS and RS held

Table 3
Parameters during temperature sweep for starch suspensions of 10–30% (w/w) concentrations.

Variety	Concentration (%)	$T_{G'_{max}}$ (°C)	G'_{max} (Pa)	$\tan \delta_{G'_{max}}$
PS	10	71.2 ± 0.9	1349 ± 48	0.28 ± 0.03
	15	69.3 ± 1.0	1731 ± 56	0.29 ± 0.02
	20	68.4 ± 1.1	2546 ± 41	0.26 ± 0.01
	30	66.9 ± 0.5	5483 ± 204	0.25 ± 0.01
CS	10	72.4 ± 1.0	416 ± 30	0.26 ± 0.01
	15	70.1 ± 0.8	1248 ± 48	0.24 ± 0.00
	20	69.5 ± 0.8	1655 ± 59	0.25 ± 0.01
	30	73.2 ± 1.1	2571 ± 26	0.20 ± 0.00
RS	10	84.4 ± 1.0	1208 ± 15	0.05 ± 0.01
	15	80.8 ± 0.5	3607 ± 50	0.05 ± 0.00
	20	76.8 ± 0.8	6122 ± 65	0.08 ± 0.00
	30	77.5 ± 1.2	14435 ± 379	0.06 ± 0.01

$T_{G'_{max}}$, temperatures at which G' reaches to its maximum during temperature sweep; G'_{max} , maximum G' during temperature sweep; $\tan \delta_{G'_{max}}$, $\tan \delta$ at G'_{max} .

yield stress (τ_y) values of 61, 102, and 191 Pa, respectively. τ_y value, which reflects that the mechanical strength of materials is crucial for supporting the subsequently deposited layers and maintaining printed shapes during the deposition process (Feilden et al., 2016; Gibiński et al., 2006). Along with our discussion about G' , the τ_y values of these starch samples were also influenced by the swollen starch granules followed by the leached amylose contained in the system. On the other hand, CS and RS displayed flow stress (τ_f) values of 484 and 3710 Pa, respectively, which were much lower than that of PS (1362 Pa). τ_f has been identified as the point where $G' = G''$, indicating the extrudability of a material during printing, which implies the force necessary for

Table 4
Parameters during alternate strains sweep experiments for different starch samples of 10–30% (w/w) concentrations.

Variety	Concentration (%)	G'_1 (Pa)	G'_2 (Pa)	G'_3 (Pa)	G'_5 (Pa)
CS	10	561	65	366	338
	20	1429	217	951	885
	30	2429	1217	1951	1885
RS	10	1039	613	845	813
	20	5357	157	3471	3115
	30	12398	270	7732	6671
PS	10	1452	733	1228	1242
	20	2224	659	1885	1764
	30	4926	2800	3797	3644

G'_1 , G' at 1% strain of the first stage; G'_2 , G' at 100% strain of the second stage; G'_3 , G' at 1% strain of the third stage; G'_5 , G' at 100% strain of the fifth stage.

extrusion. From the τ_y and τ_f results here, one can anticipate that RS present stronger mechanical properties, better printability, and higher resolutions than the other two starches, while PS, which yielded high τ_f values, might be hard to be extruded from the nozzle.

Fig. 5 (B) shows the changes in τ_y and τ_f for these three starches as a function of concentration. It can be seen that τ_y and τ_f values were both concentration-dependent, this was consistent with previous results (Evans and Haisman, 1980; Wang et al., 1994). Higher concentrations could contribute to higher τ_y values, which would lead to a better resistance to deformation and thus more stacked layers without printing defects and high resolutions of the printed structures. However, higher τ_f values also resulted from the increased concentration, which indicates that the stronger force is needed for the printing media to be

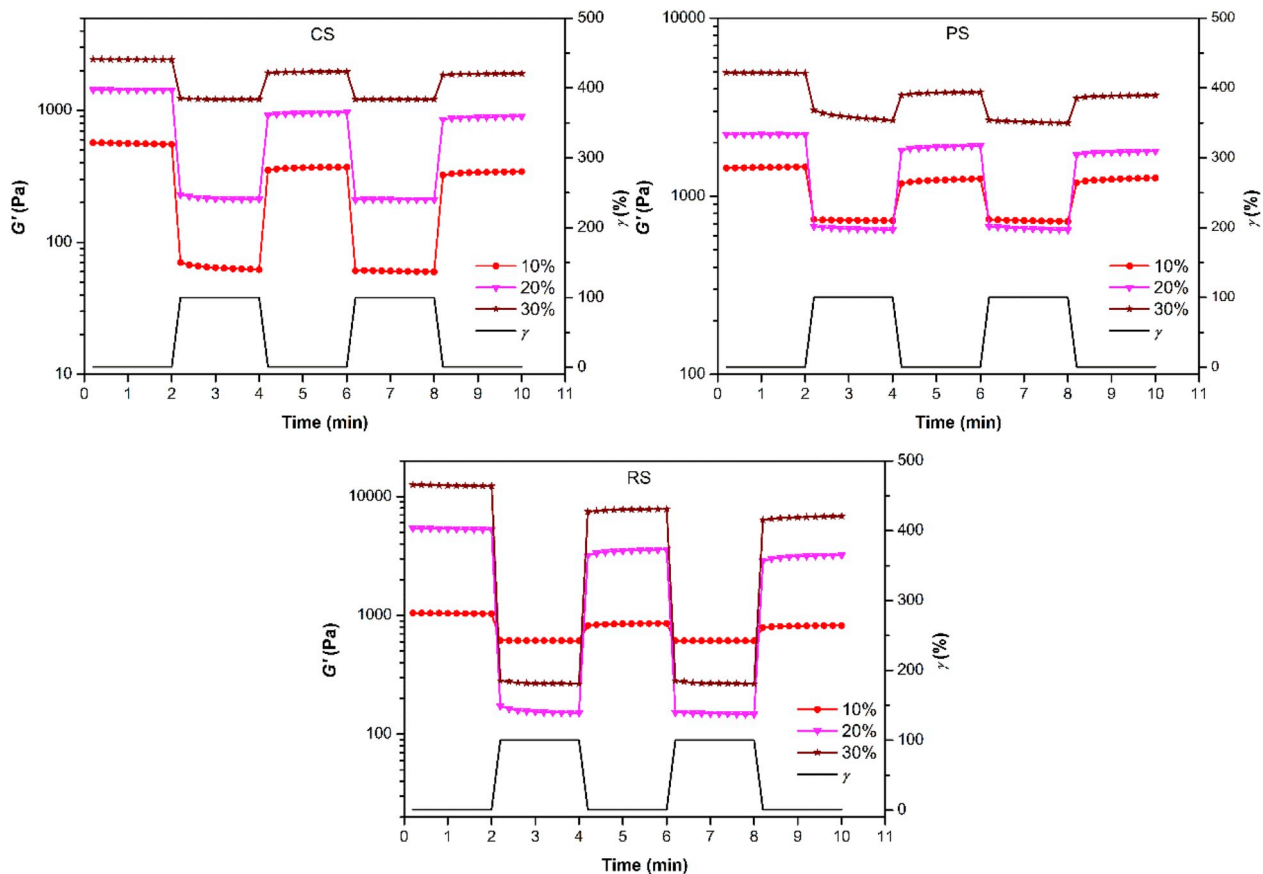


Fig. 4. Alternate strain sweep tests showing G' for CS at 75 °C, RS at 80 °C, and PS at 70 °C responsive to high (100%) and low (1%) oscillatory strains (γ).

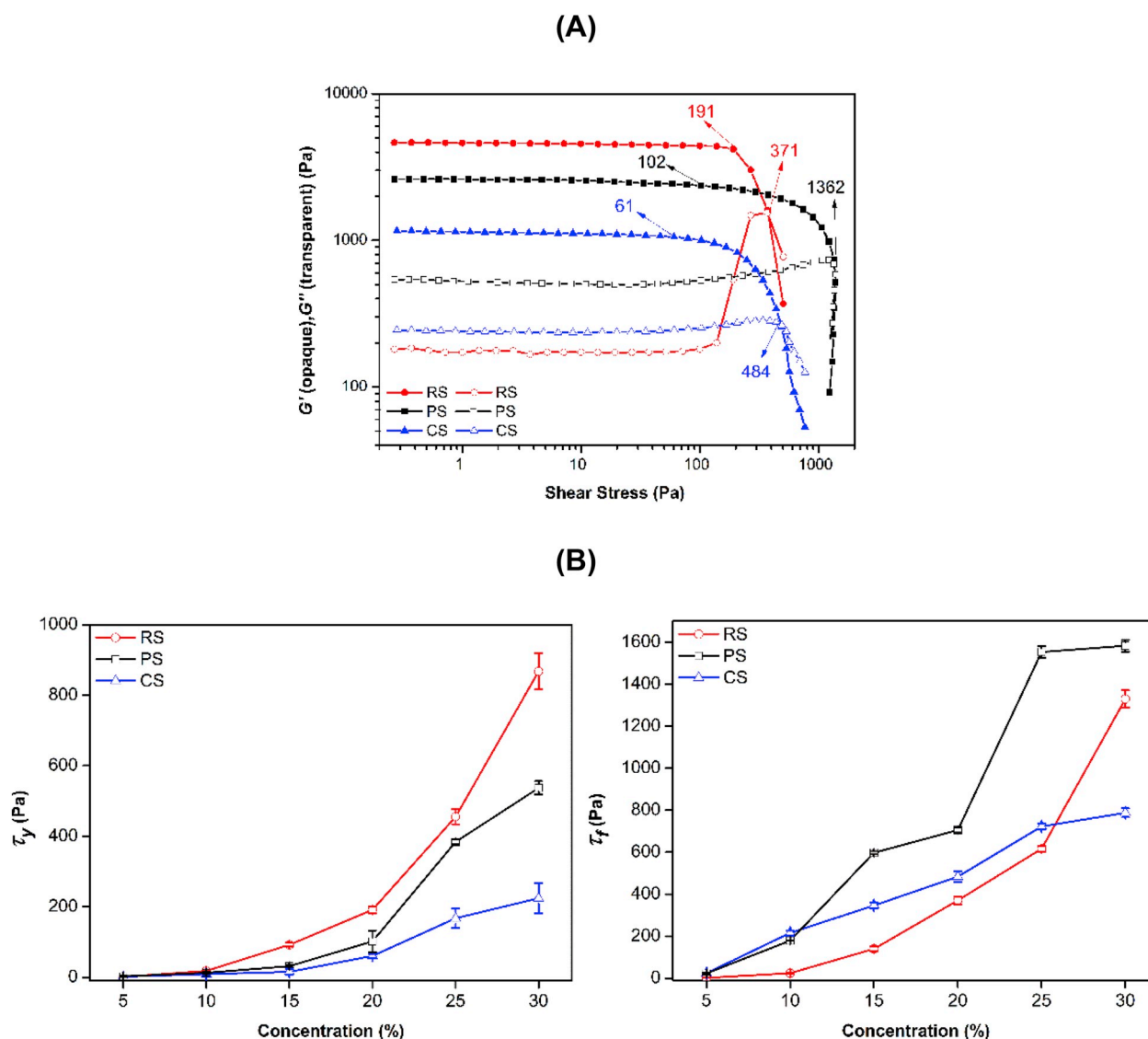


Fig. 5. Stress sweep for 20% (w/w) starches (A). Yield stress (τ_y) and flow stress (τ_f) as a function of concentration (B) for CS at 75 °C, RS at 80 °C and PS at 70 °C.

extruded from the nozzle. Regarding this, suitable concentration ranges for all three starch samples should be optimized with the considerations of the product quality and processability. This will be discussed in the next part. Besides, in the tested concentration ranges, RS had highest τ_y values and lowest τ_f values (excepted from 30% w/w), indicating that it is superior as a printed medium in a wide concentration range.

3.3. HE-3D printed objects

Fig. 6 presents the printed constructs including a smiling face (50 × 50 × 7 mm), a beetle (16 × 96 × 8 mm) and a bowl (28 × 28 × 49 mm). From all observations, all starches at 10% (w/w) and 15% (w/w) CS could be smoothly extruded from the nozzle, which could be ascribed to the low τ_f values (Fig. 5 (B)). However, these printed objects deformed immediately and showed poor resolutions because of sagging, which was due to the weak mechanical strength reflected by low τ_y (Fig. 5 (B)) and G'_3 (Table 4).

For RS, the printed constructs at 15–25% (w/w) concentrations could withstand the shape over time and displayed a smoother surface with increasing concentration. Given this, RS with τ_f (140–616 Pa), G' (2313–6909 Pa) and τ_y (92–455 Pa) were strong enough to support the deposited layers and hold the shape from the target constructs. Besides, Table 5 shows that the number of printed layers also increased, and the

printed structures exhibited a high resolution (0.804–0.972 mm line width). This was as expected since materials with suitable G' and τ_y showed better shape retention capability and high resolutions (Lewis, 2006; Zhang et al., 2015). For the printed RS objects with 30% (w/w), despite the good shape of the target constructs, they also displayed some defects and structural inconsistency throughout printing due to the broken extrudate thread. This might be due to the high τ_f value (1330 Pa), which led to the poor printability of starch gels during deposition.

Similarly, CS of 20–25% (w/w) concentrations showed favorable printability owing to the proper τ_f values (484–722 Pa). However, the shape retention and resolutions of printed constructs by CS were not as good as RS due to its weaker mechanical strength as indicated by the lower τ_y (61–167 Pa) and G' (1150–1545 Pa) values. Moreover, the 30% (w/w) CS sample was hard for extrusion during printing due to its high τ_f (788 Pa).

The printed PS constructs with concentrations 15–20% (w/w) showed preferable resolutions (0.915–0.935 mm line width) and structural consistency. Nevertheless, the number of printed layers of constructs without collapse was less than that for RS, which might be due to the lower τ_y values (32–102 Pa) of PS than those of RS. Further increasing the concentration of PS to 25 or 30% (w/w) led to τ_f (1553–1583 Pa) and G'_2 (868–2799 Pa) that were too high under a high

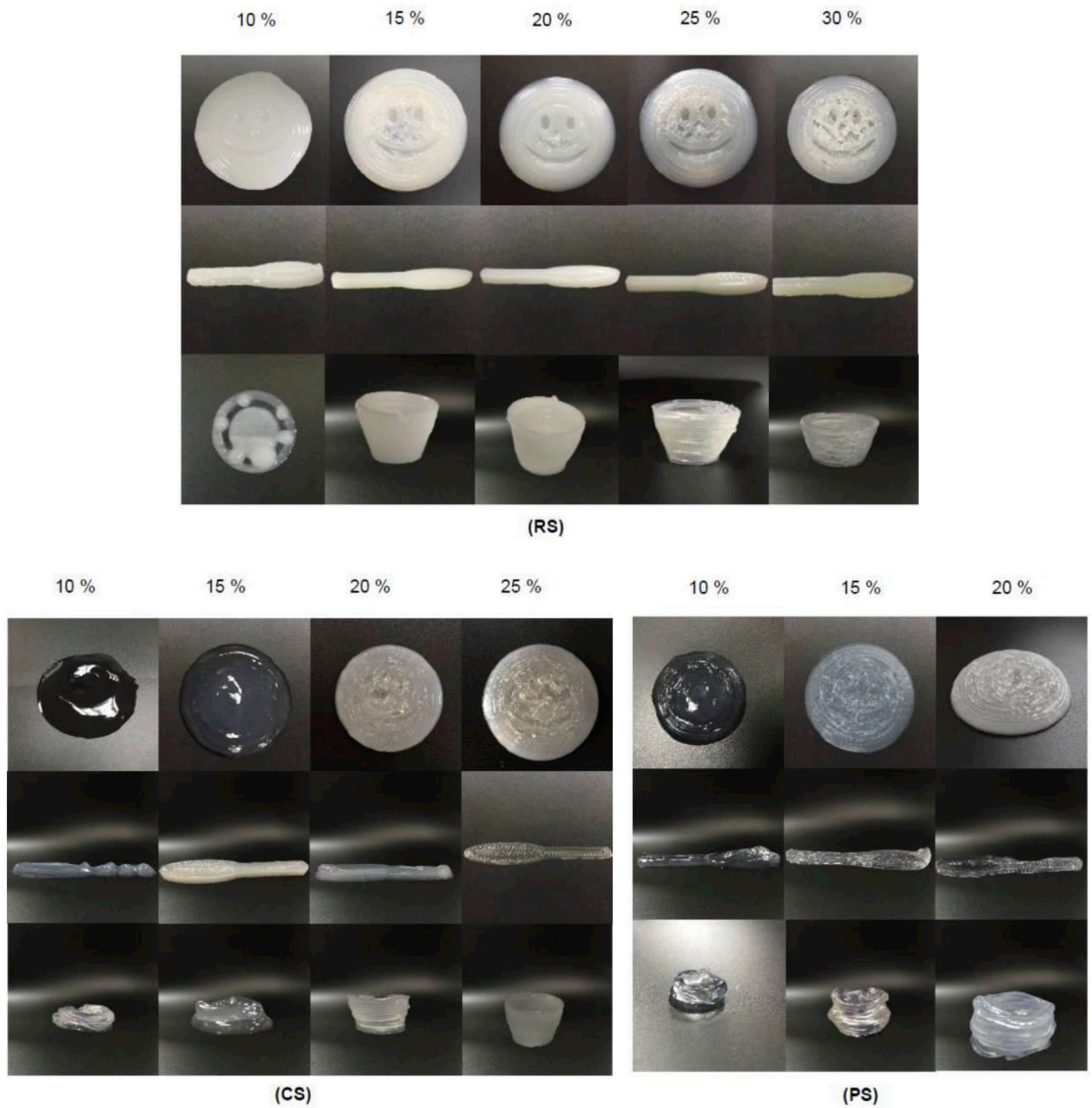


Fig. 6. HE-3D printed objects by using RS at 80 °C, CS at 75 °C and PS at 70 °C at different concentrations.

Table 5
Printed parameters for different starch of 10–30% (w/w) concentrations.

Concentration (w/w)	RS		CS		PS	
	line width (mm)	printed layer	line width (mm)	printed layer	line width (mm)	printed layer
10%	1.338 ± 0.016 ^a	3 ± 1.4 ^d	1.263 ± 0.007 ^a	1 ± 0.0 ^b	1.197 ± 0.003 ^a	3 ± 0.0 ^c
15%	0.972 ± 0.076 ^b	43 ± 1.4 ^b	1.043 ± 0.003 ^b	5 ± 1.4 ^b	0.935 ± 0.006 ^b	11 ± 1.4 ^b
20%	0.866 ± 0.008 ^{bc}	58 ± 2.8 ^a	1.024 ± 0.001 ^c	20 ± 2.8 ^a	0.915 ± 0.003 ^c	17 ± 2.8 ^a
25%	0.804 ± 0.011 ^c	60 ± 2.8 ^a	0.983 ± 0.004 ^d	16 ± 1.4 ^a	0.856 ± 0.006 ^d	2 ± 1.4 ^c
30%	0.797 ± 0.023 ^c	32 ± 1.4 ^c	NE	NE	NE	NE

NE means not extruded. Values followed by the different lowercase letter within a column differ significantly ($p < 0.05$). Values are presented as means ± SD (standard deviation) of three determinations (n = 3).

shear process through the nozzle so that PS could not be extruded from the nozzle smoothly.

4. Conclusion

This study focused on the HE-3DP of starch and we have established the relationship between rheological properties and printability. The results indicated that concentrated starches present shear-thinning and strain-responsiveness, which were printable as HE-3DP materials. Moreover, the τ_y and G' parameters of all the samples, which are crucial for supporting subsequently deposited layers and maintaining printed shapes, increased with the increased starch concentration. Nevertheless, the increased starch concentration could lead to over-high τ_f values that hindered smooth extrusion of starch materials. Thus, the highly desirable starch materials for HE-3DP should not only possess suitable τ_y and G' , which are important for printing constructs to withstand its own weight, but also have relatively low τ_f to be easily extruded out from a small-diameter nozzle. Our results indicated that RS of 15–25% (w/w) concentrations at 80 °C, CS of 20–25% (w/w) concentrations at 75 °C, and PS of 15–20% (w/w) concentration at 70 °C possessed appropriate τ_f (140–722 Pa), τ_y (32–455 Pa) and G' (1150–6909 Pa) values, which were preferable for HE-3DP with excellent printability, shape retention and resolutions. Therefore, the information obtained from this work could provide useful guidance for the selection of starch-based food materials and the optimization of 3D printing processes for developing next-generation individualized food.

Acknowledgments

This article has been financially supported by the National Key R&D Program of China (2016YFD04012021), the Key Project of Guangzhou Science and Technology Program (No.201804020036) and YangFan Innovative and Entrepreneurial Research Team Project (2014YT02S029). F. Xie acknowledges the European Union's Marie Skłodowska-Curie Actions (MSCA) and the Institute of Advanced Study (IAS), University of Warwick for the Warwick Interdisciplinary Research Leadership Programme (WIRL-COFUND).

Appendix A. Supplementary data

Supplementary data to this article can be found online at <https://doi.org/10.1016/j.jfoodeng.2018.09.011>.

References

Caldirola, P., 1962. Ferry, J. D. - viscoelastic properties of polymers. *Scientia, Rivista di Scienza* 56 (97), 179.

Chen, X., Liu, P., Shang, X., Xie, F., Jiang, H., Wang, J., 2017. Investigation of rheological properties and conformation of cassava starch in zinc chloride solution. *Starch - Stärke* 69 (9–10), 1600384.

Chung, J.H.Y., Naficy, S., Yue, Z., Kapsa, R., Quigley, A., Moulton, S.E., Wallace, G.G., 2013. Bio-ink properties and printability for extrusion printing living cells. *Biomaterials Science* 1 (7), 763.

Cohen, D.L., Lipton, J.L., Cutler, M., Coulter, D., Vesco, A., Lipson, H., 2009. Hydrocolloid Printing: a Novel Platform for Customized Food Production. *Solid Freeform Fabrication Symposium*. Austin, TX. pp. 807–818.

Duoss, E.B., Weisgraber, T.H., Hearon, K., Zhu, C., IV, W.S., Metz, T.R., Vericella, J.J., Barth, H.D., Kuntz, J.D., Maxwell, R.S., Spadaccini, C.M., Wilson, T.S., 2014. Three-dimensional printing of elastomeric, cellular architectures with negative stiffness. *Adv. Funct. Mater.* 24 (31), 4905–4913.

Evans, I.D., Haisman, D.R., 1980. Rheology of gelatinised starch suspensions. *J. Texture Stud.* 10 (4), 347–370.

Feilden, E., Blanca, E.G.T., Giuliani, F., Saiz, E., Vandeperre, L., 2016. Robocasting of structural ceramic parts with hydrogel inks. *J. Eur. Ceram. Soc.* 36 (10), 2525–2533.

Gibiński, M., Kowalski, S., Sady, M., Krawontka, J., Tomasik, P., Sikora, M., 2006. Thickening of sweet and sour sauces with various polysaccharide combinations. *J. Food Eng.* 75 (3), 407–414.

Hao, L., Mellor, S., Seaman, O., Henderson, J., Sewell, N., Sloan, M., 2010. Material characterisation and process development for chocolate additive layer manufacturing. *Virtual Phys. Prototyp.* 5 (2), 57–64.

Hong, S., Sycks, D., Chan, H.F., Lin, S., Lopez, G.P., Guilak, F., Leong, K.W., Zhao, X., 2015. 3D printing of highly stretchable and tough hydrogels into complex, cellularized structures. *Adv. Mater.* 27 (27), 4035–4040.

Jafari, M.A., Han, W., Mohammadi, F., Safari, A., Danforth, S.C., Langrana, N., 2000. A novel system for fused deposition of advanced multiple ceramics. *Rapid Prototyp. J.* 6 (3), 161–175.

Ji, Z., Yu, L., Liu, H., Bao, X., Wang, Y., Chen, L., 2017. Effect of pressure with shear stress on gelatinization of starches with different amylose/amylopectin ratios. *Food Hydrocolloids* 72, 331–337.

Keetels, C., Van Vliet, T.P.W., 1996. Gelation and retrogradation of concentrated starch systems: 1 Gelation. *Food Hydrocolloids* 10 (3), 343–353.

Kokkinis, D., Schaffner, M., Studart, A.R., 2015. Multimaterial magnetically assisted 3D printing of composite materials. *Nat. Commun.* 6, 8643.

Lanaro, M., Forrestal, D.P., Scheurer, S., Slinger, D.J., Liao, S., Powell, S.K., Woodruff, M.A., 2017. 3D printing complex chocolate objects: platform design, optimization and evaluation. *J. Food Eng.* 215, 13–22.

Le Tóhic, C., O'Sullivan, J.J., Drapala, K.P., Chartrin, V., Chan, T., Morrison, A.P., Kerry, J.P., Kelly, A.L., 2018. Effect of 3D printing on the structure and textural properties of processed cheese. *J. Food Eng.* 220, 56–64.

Lewis, J.A., 2006. Direct ink writing of 3D functional materials. *Adv. Funct. Mater.* 16 (17), 2193–2204.

Li, J.Y., Yeh, A.L., 2001. Relationships between thermal, rheological characteristics and swelling power for various starches. *J. Food Eng.* 50 (3), 141–148.

Lii, C., Shao, Y., Tseng, K., 1995. Gelation Mechanism and rheological properties of rice starch. *Cereal Chem.* 72 (4), 393–400.

Lii, C.Y., Tsai, M.L., Tseng, K.H., 1996. Effect of amylose content on the rheological property of rice starch. *Cereal Chem.* 73 (4), 415–420.

Lipton, J., Arnold, D., Nigl, F., Lopez, N., Cohen, D., Norén, N., Lipson, H., 2010. Multi-material Food Printing with Complex Internal Structure Suitable for Conventional Post-processing. *Solid Freeform Fabrication Symposium*. pp. 809–815.

Liu, Z., Zhang, M., Bhandari, B., Yang, C., 2018. Impact of rheological properties of mashed potatoes on 3D printing. *J. Food Eng.* 220, 76–82.

Long, J., Gholizadeh, H., Lu, J., Bunt, C., Seyfoddin, A., 2017. Application of fused deposition modelling (FDM) method of 3D printing in drug delivery. *Curr. Pharmaceut. Des.* 23 (3), 433–439.

Ring, S.G., 1985. Some studies on starch gelation. *Starch - Stärke* 37 (3), 80–83.

Serizawa, R., Shitara, M., Gong, J., Makino, M., Kabir, M.H., Furukawa, H., 2014. 3D Jet Printer of Edible Gels for Food Creation, SPIE Smart Structures And Materials + Nondestructive Evaluation And Health Monitoring. SPIE, pp. 6.

Shaw, M.T., 2011. Relationship between Stress and Rate of Deformation: the Newtonian Fluid, Introduction To Polymer Rheology. John Wiley & Sons, Inc., pp. 59–70.

Singh, N., Singh, J., Kaur, L., Singh Sodhi, N., Singh Gill, B., 2003. Morphological, thermal and rheological properties of starches from different botanical sources. *Food Chem.* 81 (2), 219–231.

Sun, J., Zhou, W., Huang, D., Fuh, J.Y.H., Hong, G.S., 2015. An overview of 3D printing technologies for food fabrication. *Food Bioprocess Technol.* 8 (8), 1605–1615.

Suzlin, T., Fengwei, X., Timothy, M.N., Peng, L., Peter, J.H., 2011. Rheological properties of thermoplastic starch studied by multipass rheometer. *Carbohydr. Polym.* 83 (2), 914–919.

Svegmark, K., Hermansson, A.-M., 1991. Changes induced by shear and gel formation in the viscoelastic behaviour of potato, wheat and maize starch dispersions. *Carbohydr. Polym.* 15 (2), 151–169.

Tsai, M.L., Li, C.F., Lii, C.Y., 1997. Effects of granular structures on the pasting behaviors of starches. *Cereal Chem.* 74 (6), 750–757.

Wang, S., Chao, C., Xiang, F., Zhang, X., Wang, S., Copeland, L., 2018. New insights into gelatinization mechanisms of cereal endosperm starches. *Sci. Rep.* 8 (1), 3011.

Wang, S.S., Qu, D., Chiew, Y.C., 1994. A study of starch granular aggregation. *Starch - Stärke* 46 (9), 337–341.

Wegrzyn, T.F., Golding, M., Archer, R.H., 2012. Food layered manufacture: a new process for constructing solid foods. *Trends Food Sci. Technol.* 27 (2), 66–72.

Winnik, M.A., Yekta, A., 1997. Associative polymers in aqueous solution. *Curr. Opin. Colloid Interface Sci.* 2 (4), 424–436.

Wong, R.B.K., Lelievre, J., 1981. Viscoelastic behaviour of wheat starch pastes. *Rheol. Acta* 20 (3), 299–307.

Xie, W., Shao, L., 2009. Phosphorylation of corn starch in an ionic liquid. *Starch - Stärke* 61 (12), 702–708.

Yang, F., Zhang, M., Bhandari, B., 2017. Recent development in 3D food printing. *Crit. Rev. Food Sci. Nutr.* 57 (14), 3145–3153.

Yang, F., Zhang, M., Bhandari, B., Liu, Y., 2018. Investigation on lemon juice gel as food material for 3D printing and optimization of printing parameters. *LWT - Food Sci. Technol. (Lebensmittel-Wissenschaft - Technol.)* 87, 67–76.

Zhang, M., Vora, A., Han, W., Wojtecki, R.J., Maune, H., Le, A.B.A., Thompson, L.E., McClelland, G.M., Ribet, F., Engler, A.C., Nelson, A., 2015. Dual-responsive hydrogels for direct-write 3D printing. *Macromolecules* 48 (18), 6482–6488.

Zheng, B., Wang, H., Shang, W., Xie, F., Li, X., Chen, L., Zhou, Z., 2018. Understanding the digestibility and nutritional functions of rice starch subjected to heat-moisture treatment. *Journal of Functional Foods* 45, 165–172.